ECMWF Analyses and Reanalyses Depiction of ENSO Signal in Antarctic Precipitation*

DAVID H. BROMWICH+ AND ARIC N. ROGERS
Polar Meteorology Group, Byrd Polar Research Center, The Ohio State University, Columbus, Ohio

PER KÅLLBERG
European Centre for Medium-Range Weather Forecasts, Shinfield Park, Reading, United Kingdom

RICHARD I. CULLATHER
Department of Aerospace Engineering Sciences, University of Colorado, Boulder, Colorado

JAMES W. C. WHITE
Institute of Arctic and Alpine Research, University of Colorado, Boulder, Colorado

KARL J. KREUTZ#
Climate Change Research Center, Institute for the Study of Earth, Oceans and Space, University of New Hampshire, Durham, New Hampshire

(Manuscript received 1 February 1999, in final form 21 June 1999)

ABSTRACT

The El Niño–Southern Oscillation (ENSO) signal in Antarctic precipitation is evaluated using European Centre for Medium-Range Weather Forecasts (ECMWF) operational analyses and ECMWF 15-yr (1979–93) reanalyses. Operational and reanalysis datasets indicate that the ENSO teleconnection with Antarctic precipitation is manifested through a close positive correlation between the Southern Oscillation index and West Antarctic sector (75°–90°S, 120°W–180°) precipitation from the early 1980s to 1990, and a close negative correlation after 1990. However, a comparison between the operational analyses and reanalyses shows significant differences in net precipitation ($P - E$) due to contrasts in the mean component of moisture flux convergence into the West Antarctic sector. These contrasts are primarily due to the mean winds, which differ significantly between the operational analyses and the reanalyses for the most reliable period of overlap (1985–93). Some of the differences in flow pattern are attributed to an error in the reanalysis assimilation of Vostok station data that suppresses the geopotential heights over East Antarctica. Reanalysis geopotential heights are also suppressed over the Southern Ocean, where there is a known cold bias below 300 hPa. Deficiencies in ECMWF reanalyses result in a weaker ENSO signal in Antarctic precipitation and cause them to miss the significant upward trend in precipitation found in recent operational analyses. Ice-core analyses reflect both an upward trend in ice accumulation and the ENSO teleconnection correlation pattern seen in the operational analyses. This study confirms the results of a previous study using ECMWF operational analyses that was the first to find a strong correlation pattern between the moisture budget over the West Antarctic sector and the Southern Oscillation index.

1. Introduction

In remote areas of the high southern latitudes, the information obtained by direct measurements of atmospheric and surface parameters is limited not only by the accuracy of the collection methods employed but also by the sparcity of the observational network in place. The goal of seeking an accurate representation of the spatial and temporal variability of precipitation over the Antarctic continent is governed by these limitations, as are other climatological studies (Bromwich 1988; Bromwich et al. 1998). Expectations from the International Trans-Antarctic Scientific Expedition (ITASE), a project that will use ice-core data to obtain annual

* Byrd Polar Research Center Contribution Number 1142.
+ Additional affiliation: Atmospheric Sciences Program, Department of Geography, The Ohio State University, Columbus, Ohio.
# Current affiliation: Department of Marine Chemistry and Geochemistry, Woods Hole Oceanographic Institution, Woods Hole, Massachusetts.

Corresponding author address: David H. Bromwich, Polar Meteorology Group, Byrd Polar Research Center, The Ohio State University, 1090 Carmack Rd., Columbus, OH 43210-1002.
E-mail: bromwich@polarmet1.mps.ohio-state.edu

temporal resolution over a significant portion of the Antarctic continent, heighten interest in the potential of using atmospheric numerical analyses to reproduce snow accumulation patterns and their temporal variability. Snow accumulation closely approximates precipitation minus evaporation/sublimation ($P - E$) over most parts of Antarctica. Global analysis models allow the atmosphere to be studied with a rigor that would be extremely difficult and expensive to match using direct observational approaches. Use of numerical analyses to estimate high–southern latitude precipitation is described by Yamazaki (1992), Bromwich et al. (1995), Genthon and Braun (1995), Budd et al. (1995), Cullather et al. (1996), and Cullather et al. (1998).

Despite the obvious benefits, caution must be exercised when using model analyses. A comparison with available observations is necessary in order to establish numerical analysis integrity. This study makes extensive use of available observations to establish the validity of numerical analyses in climatological research and addresses the issue of conflicting results from European Centre for Medium-Range Weather Forecasts (ECMWF) operational analyses and the 15-yr reanalyses related to recent interannual variability and trends in Antarctic precipitation. Previously, Cullather et al. (1996, hereinafter C96) presented a review of literature relating atmospheric circulation over Antarctica to the El Niño–Southern Oscillation (ENSO) phenomenon. In C96 $P - E$ is computed via the atmospheric moisture budget using operational analyses from ECMWF. Values for the South Pacific sector of West Antarctica bounded by 75°–90°S, 120°W–180° are found to be correlated with ENSO from the early 1980s through 1990. The relation becomes anticorrelated after 1990, a period corresponding to a significant increase in $P - E$ for the Antarctic continent.

A recent study by Genthon and Krinner (1998, hereinafter GK98) using the ECMWF 15-yr reanalyses (ERA-15) found fundamental differences with results of C96 using ECMWF operational analyses. GK98 state that they are unable to find a strong ENSO signal in West Antarctic precipitation, and results using ERA-15 do not indicate a significant upward trend in $P - E$ for the Antarctic continent over the reanalysis time period. It is suggested by GK98 that spurious trends in the operational analyses may be the reason for the discrepancies they find. This conclusion conflicts with prior validation studies of the ECMWF operational analyses in high southern latitudes (e.g., Bromwich et al. 1995; Cullather et al. 1997). Although some differences among the datasets are expected (and even desired), the degree of discrepancy between them warrants serious consideration. The need for validation of the new dataset is even more necessary given the comprehensive validation that has already been done in the studies listed above using ECMWF operational data.

The conflicting results also raise concerns regarding the true nature of the high–southern latitude ENSO teleconnection. These concerns are particularly important in the context of recent studies showing Antarctic sea-ice variability related to ENSO (Gloersen 1995; Simmonds and Jacka 1995), oceanic circumpolar variability on ENSO timescales (White and Peterson 1996), increased frequency of South Pacific blocking related to the ENSO warm phase (Renwick 1998), and high-latitude connections to tropical South Pacific warm and cold events linked by climate anomaly wave train patterns (Houseago et al. 1998). There is also a study using observational data from the early 1980s through the middle 1990s showing a possible ENSO signal in the Ross Sea (Ledley and Huang 1997). A statistically significant relationship is found between sea surface temperatures in the Ross Sea (which includes part of the West Antarctic sector used in C96 and in this study) and ENSO variations. Understanding the ENSO teleconnection with high southern latitudes will lead to better seasonal forecasting. The importance of seasonal forecasting is not lost on U.S. Antarctic field researchers from the austral summer of 1997–98 (one of the most intense ENSO periods of the century) for the Ross Ice Shelf and West Antarctic regions. They experienced unusually severe weather conditions resulting in curtailment of field activities and a late opening of Amundsen–Scott Station (South Pole). In addition, unusual storminess over the Ross Sea forced an early end to sediment-core retrieval efforts of the Cape Roberts project (Stone 1997).

The following sections of this paper critically evaluate ECMWF operational analyses and the results of C96 in comparison with ERA-15 data and in situ observations. The $P - E$ estimates of C96 are also updated to include data through March of 1999. $P - E$ estimates and mean field differences between ERA-15 and operational analyses are discussed in section 3. Analysis validation using available observations is covered in section 4. This section also uses analyses of West Antarctic sector ice cores to substantiate tendencies in precipitation accumulation and West Antarctic sector teleconnections with ENSO. Conclusions regarding analysis integrity and the impact of analysis/observation differences are discussed in section 5.

2. Numerical analysis descriptions

Three ECMWF numerical analysis data archives are used to compute $P - E$ in this study. Two of the archives consist of operational analyses. The first of these, the World Meteorological Organization (WMO) archive, is made up of initialized analyses that span 1980–89. The second operational dataset is composed of uninitialized analyses from the World Climate Research Programme/Tropical Oceans Global Atmosphere (WCRP/TOGA) Archive II and spans 1985–99. These two operational datasets are in reality based on the same operational analyses, the only difference between them being that one of them is initialized. The third ECMWF dataset,

ERA-15, is a 15-yr reanalysis (see Gibson et al. 1997, and references therein) that runs from 1979 to 1993. Both operational datasets consist of analyses every 12 h at 0000 and 1200 UTC. ERA-15 analyses are available four times daily. All analyses are archived on a 2.5° latitude–longitude grid. The WMO operational analyses consist of data at seven standard pressure levels to 100 hPa. The WCRP/TOGA (hereafter referred to as TOGA) operational analyses include 14 standard pressure levels and the ERA-15 dataset includes 17 standard pressure levels to 10 hPa. Although the vertical resolutions of the datasets differ, the same levels are used in both ERA-15 and TOGA $P - E$ calculations for consistency. All these ECMWF products are obtained from the National Center for Atmospheric Research.

Although both WMO and TOGA operational analyses are used to estimate West Antarctic sector precipitation, the TOGA archive is the most current and so includes the latest assimilation scheme enhancements available. Thus, it is used extensively throughout this paper in comparisons with the ERA-15 archive and in numerical analysis validation efforts using observations. Details regarding changes made to the production methods of both operational analysis datasets can be found in Trenberth (1992). However, one of the more noteworthy changes to the analysis production method occurs in September 1991 when an increase in model resolution is implemented along with changes to horizontal and vertical diffusion, advection, and clouds.

The concept of reanalyses is popular because of consistent assimilation procedures and maximum observation usage. Thus, unlike operational analyses, ERA-15 does not suffer from discontinuities that occur as a result of assimilation scheme changes. In addition, data from the Global Telecommunications System that are deemed worthy of inclusion in analysis production, but that are not transmitted in time for use in TOGA operational analyses, are used in ERA-15.

Another major and important difference between the operational analyses and those in ERA-15 is how TIROS Operational Vertical Sounder (TOVS) soundings from polar-orbiting satellites are used. During most of the ''WMO–TOGA'' years, ECMWF operations used the National Environmental Satellite Data and Information Service statistical retrievals, often referred to as ''SATEMs.'' They have a low spatial (~500 km) resolution and are unable to describe the vertical structure of the troposphere with great detail. In ERA-15 the TOVS data are used in the form of cloud cleared radiances (CCR) that are assimilated with the 1D-Var technique (see section 4 below). These data have a much higher spatial resolution and they have a larger impact on the analyses than the SATEMs.

3. Comparison of ERA-15 and TOGA moisture flux and analysis fields

a. Moisture flux convergence analysis

Moisture flux convergence (MFC) is an estimation of precipitation minus evaporation/sublimation from numerical analyses using the atmospheric moisture budget (e.g., Yamazaki 1992). Excluding storage term changes in precipitable water, which are found to be small on interannual timescales, the spatially and temporally averaged atmospheric moisture budget may be expressed as

$$\langle \overline{P} - \overline{E} \rangle = -\frac{1}{A} \oint \left(\int_0^{P_{\text{sfc}}} \frac{\overline{q\mathbf{V}}}{g}\, dp \right) \cdot \mathbf{n}\, dl \qquad (1)$$

following C96, where P is the precipitation rate, E is the rate of evaporation/sublimation, A is the area over which the net precipitation is calculated, g is gravity, q is specific humidity, P_{sfc} is the surface pressure, $\mathbf{V}$ is the horizontal wind field, and $\mathbf{n}$ is the outward normal to the area perimeter. It is computed for the aforementioned west Antarctic sector bounded by 75°–90°S, 120°W–180° (Fig. 1). A complete discussion of MFC calculations, as well as the reasons for choosing this sector for study, can be found in C96. However, the primary reason for focusing on this sector is because of the high frequency of cyclonic activity in this region and associated high annual precipitation.

Figure 2 shows the computed annual running mean MFCs (from monthly values) of the WMO and TOGA operational analyses updated from C96 through March of 1999. Annual running mean Southern Oscillation index (SOI) values, obtained from the Climate Prediction Center, are included to show the correlation with ENSO. The period under study includes two well-defined cold events (1988/89 and 1996, SOI > 0) and at least four warm events (1982/83, 1986/87, an extended event be-

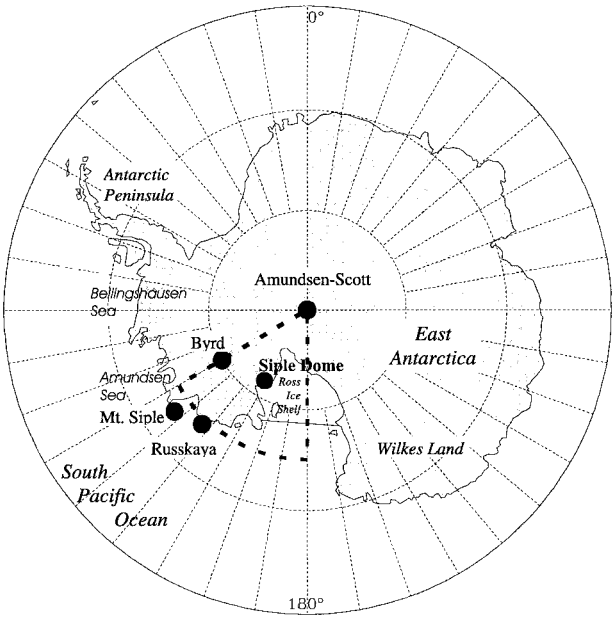

FIG. 1. Antarctic continent with the West Antarctic moisture convergence sector indicated by dashed lines (adapted from Cullather et al. 1996).

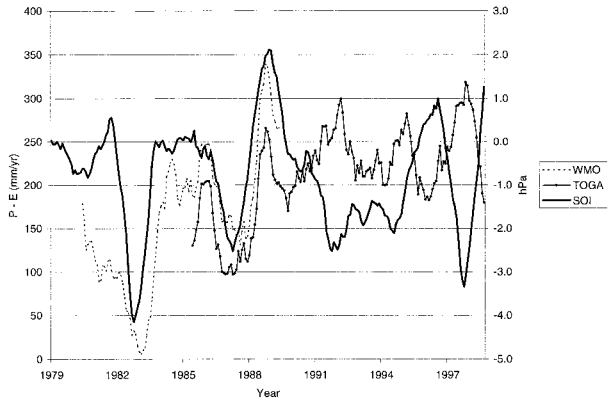

FIG. 2. Annual running mean of MFC for West Antarctic sector calculated from WMO and TOGA (updated through March of 1999) data along with the SOI.

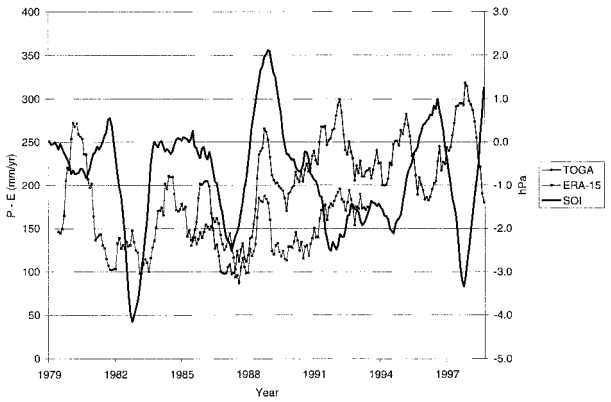

FIG. 3. Annual running mean of MFC for West Antarctic sector calculated from TOGA and ERA-15 data along with the SOI.

ginning in 1991 with varying intensity through 1995, and 1997/98, SO1 < 0). Figure 3 is similar to Fig. 2 except that the WMO MFC series is replaced by the ERA-15 series. Each of the MFC series exhibit similar correlation characteristics with the SOI, with the strongest SOI–MFC correlation pattern seen in the TOGA series. From near the beginning of the period until 1990, MFC and the SOI are positively correlated, with increases in the SOI matched by increases in total MFC values, while decreases in the SOI are reflected by dryer periods in the MFC. After 1990, the sign of correlation between MFC and the SOI switches, becoming negative. This change in correlation is noted in C96, and the strength of the post-1990 correlation pattern is substantiated by the updated series. Analysis of 500-hPa geopotential height patterns reveals that strong East Antarctic ridging begins at the time of the correlation switch (C96). This switch also occurs just before the onset of the extended ENSO event(s) beginning in 1991 (Trenberth and Hoar 1996).

To assess the relative strength of the ENSO teleconnection with West Antarctic sector MFC, correlation analyses are performed over the period when both ERA-15 and TOGA operational analyses are available (1985–93). Each series of annual running mean data (at monthly intervals) is divided at the time of the correlation switch to create two new series (pre- and post-1990). The annual running mean values are used in order to place more emphasis on the interannual relationships that exist. Finally, each series is detrended to remove multiannual trends in precipitation that obscure the correlation related to interannual variability. For 1985–90, the TOGA–SOI correlation is 0.84, and the ERA-15–SOI correlation is 0.63. The value of 0.84 for TOGA–SOI series differs slightly from the value of 0.88 quoted in C96 due to the extra step of detrending that is done here. For 1990–93, the correlation values are -0.75 and -0.74 for the TOGA–SOI and ERA-15–SOI series, respectively. The correlation values quoted above are impressive, yet it is important to determine the statistical significance due to the relatively short period for which the series overlap. This can be determined only once an effective number of independent variables is established. This number will be smaller than the number of data points in the series as a result of autocorrelation, which is common in meteorological time series and is induced by using running means. An estimate of the effective number of independent observations is obtained using the technique outlined by Angell (1981; see also Quenouille 1952, p. 168). It is given by

$$N/(1 + 2a_1b_1 + 2a_2b_2 + \cdots), \qquad (2)$$

where N is the original number of points in each of the two series, a and b. Series subscripts represent the lag-level autocorrelations. For example, a_2 is the correlation value of series a and its lag-two series. For 1985–90, N is 56 (a centered running mean starts in the middle of 1985). The lag-one autocorrelations for the SOI, TOGA, and ERA-15 series for this period are 0.981, 0.953, and 0.886, respectively. For the lag-six autocorrelations the values are 0.492, 0.307, and 0.070, respectively. Although contributions to the denominator in Eq. (2) are small at this point for any combination of two series, we carried this process out to lag-eight autocorrelations. By this point, no product of any two eight-lagged autocorrelations was greater than 0.025, resulting in less than a 0.05 contribution to the denominator in Eq. (2). The resulting effective number of independent observations is seven for the TOGA–SOI series and nine for the ERA-15–SOI series for the period 1985–90. Based on these and the correlation values quoted above, it is found that the TOGA–SOI correlation for 1985–90 is significant at nearly the 99% confidence level. The ERA-15–SOI correlation for the same period is significant at slightly greater than the 90% confidence level (typically, a value of 95% or greater is considered statistically significant using a two-tailed t test). The post-1990 overlap period between ERA-15 and TOGA operational analyses is characterized by similar MFC–SOI correlation coefficients and by shorter series. Thus, analyses of correlation and statistical sig-

nificance for TOGA–SOI variability using annual running mean data from 1990 through most of 1998 (these centered running means include data through March 1999) are performed to test the correlation stability seen in the 1990–93 series. Again, the series are detrended. The effective number of independent observations is found to be 15. The TOGA–SOI correlation value is -0.72, significant at greater than the 99% confidence level.

In a comparison with the MFC calculations presented by C96, GK98 comment on a rather disappointing lack of correlation with the SOI when ERA-15 running mean MFC values are used (although no correlation statistics are actually quoted in their study). The plot of ERA-15 annual running mean MFC (Fig. 11 in GK98) appears to be nearly identical to the ERA-15 MFC calculated in this study in Fig. 3. GK98 note that, while the ENSO events (revealed by minima in the SOI) of 1983 and 1987 do correspond with low ERA-15 net precipitation periods, the lowest net precipitation period (late 1990 in their Fig. 11) occurs a year before the third event (1991–92). GK98 go on to state that there are even periods when high SOI values are matched by low precipitation amounts. It is difficult to tell from their discussion whether they acknowledge the correlation switch that occurs in 1990, as discussed in C96 and which is of great importance to the correlation analysis.

Although the ERA-15 MFC series variability is correlated with the SOI, the correlation is not as strong and the variability is somewhat damped relative to the TOGA operational MFC. In addition, the reanalyses lack a distinctive precipitation trend, whereas the TOGA operational depiction shows a significant upward trend in precipitation through the period. The MFC discrepancy is especially evident in the early 1990s, near the end of the reanalysis period. Section 3b looks at the main source of the difference by exploring the individual components of MFC.

b. Eddy and mean components of MFC across the boundaries

To better understand how ENSO warm and cold events affect MFC for the West Antarctic sector outlined in Fig. 1, as well as some of the differences between the ECMWF operational and reanalysis products, it is necessary to look more closely at the individual (annual running mean) components that contribute to MFC.

The mean and eddy components of atmospheric moisture transport may be separated using

$$\overline{q\mathbf{V}} = \overline{q}\,\overline{\mathbf{V}} + \overline{q'\mathbf{V}'}, \tag{3}$$

where prime denotes a departure from the monthly time average. We can now write Eq. (1) as

$$\langle \overline{P} - \overline{E} \rangle = -\frac{1}{A}\Bigg[\overbrace{\oint \left(\int_0^{P_{\rm sfc}} \frac{\overline{q}\,\overline{\mathbf{V}}}{g}\,dp\right)\cdot\mathbf{n}\,dl}^{X} + \overbrace{\oint \left(\int_0^{P_{\rm sfc}} \frac{\overline{q'\mathbf{V}'}}{g}\,dp\right)\cdot\mathbf{n}\,dl}^{Y}\Bigg]. \tag{4}$$

Here, the formula for MFC is written in terms of the mean (X) and eddy (Y) components.

C96 found that mean and eddy transports are of similar magnitude in West Antarctica, consistent with Lettau (1969). Figure 4 shows the total eddy contribution of MFC (again, in annual running means of monthly values) to the West Antarctic sector derived from the TOGA operational and ERA-15 datasets plotted for the period that they overlap (1985–93). Here, it is apparent that the series demonstrate a high level of agreement and that the eddy portion of MFC is fairly constant relative to large interannual fluctuations seen in the total MFC. Thus, both the discrepancy between operational and reanalysis datasets and the sharp interannual variations in total MFC must stem from the mean portion of MFC.

To evaluate the mean component of MFC, we decompose the boundary components of the X term in Eq. (4), so that

$$\begin{aligned}\oint \left(\int_0^{P_{\rm sfc}} \frac{\overline{q}\,\overline{\mathbf{V}}}{g}\,dp\right)\cdot\mathbf{n}\,dl &= -\int_{\partial N}\left(\int_0^{P_{\rm sfc}} \frac{\overline{q}\,\overline{v}}{g}\,dp\right)dl - \int_{\partial E}\left(\int_0^{P_{\rm sfc}} \frac{\overline{q}\,\overline{u}}{g}\,dp\right)dl \\ &\quad + \int_{\partial W}\left(\int_0^{P_{\rm sfc}} \frac{\overline{q}\,\overline{u}}{g}\,dp\right)dl.\end{aligned} \tag{5}$$

Here, the integral is broken into the north, east, and west component contributions, respectively. The north and east boundary integrals have negative signs in front due to the sign convention of the winds [negative meridional (v) winds imply northerly flow, and negative zonal (u) winds imply easterly flow].

Figure 5 shows the north mean component of MFC calculated from the TOGA operational and ERA-15 archives plotted against the SOI. East and west components are summed in Fig. 6 in order to directly compare

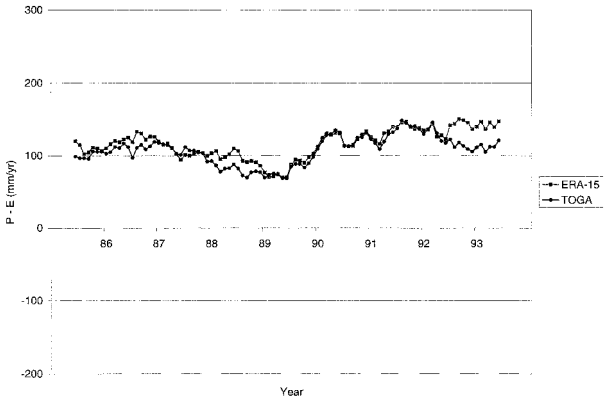

FIG. 4. Annual running mean of the eddy contribution of ERA-15 and TOGA MFC to the West Antarctic sector.

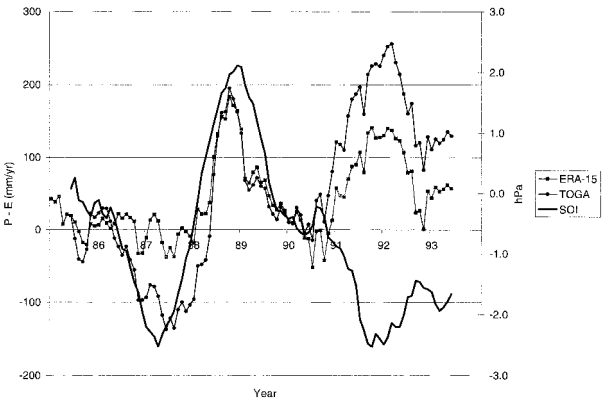

FIG. 5. Annual running mean of the mean north component of ERA-15 and TOGA MFC to the West Antarctic sector plotted with the SOI.

mean zonal components as the mean meridional (north) components are compared in Fig. 5. Depictions from both analysis datasets show that the north component of mean moisture flux into the region exhibits the greatest interannual variation. It is apparent that the sum of east and west component mean moisture fluxes offsets some of the variation seen in the north component. A closer look reveals important differences between the moisture flux components derived from TOGA operational analyses and those from ERA-15.

The north components of mean MFC to the West Antarctic sector in Fig. 5 show general agreement between the TOGA operational and the ERA-15 series in tendency through most of the period. However, the peaks and troughs of the ERA-15 series are somewhat damped when compared with those derived from TOGA analyses, especially in 1987/88 and in the early 1990s. Comparison with the SOI reveals the same correlation pattern as is found when the SOI is compared with the total MFC series in Figs. 2 and 3. A direct comparison of the magnitude of the north components of MFC does not yield a series discrepancy that is sufficient to explain all of the large differences seen in total MFC between the TOGA operational analyses and ERA-15 through the period. The periods where almost no discrepancy exists between the ERA-15 and TOGA north mean component series are generally periods when discrepancy between the zonal component series of MFC in Fig. 6 is large. Here, a significant discrepancy exists in the middle to late 1980s, with the TOGA operational series equal to or greater than the ERA-15 series. The differences in total MFC result mostly from differences in the mean zonal components prior to the SOI–MFC correlation switch circa 1990, and mostly from differences in the mean meridional components after the switch. Further MFC analysis is looked at next to determine whether moisture or atmospheric flow characteristics are more important in determining differences across the boundaries.

As a means of measuring the relative contributions of both atmospheric moisture content and atmospheric flow to the MFC, the mean component of MFC across each boundary of the West Antarctic sector is divided by the respective mean boundary value of vertically integrated specific humidity. These quantities may be written for each boundary in the following manner:

$$\text{north} = -\frac{\displaystyle\int_{\partial N}\left(\int_0^{P_{\text{sfc}}} \overline{q}\,\overline{v}\; dp\right) dl}{\displaystyle\int_{\partial N}\left(\int_0^{P_{\text{sfc}}} \overline{q}\; dp\right) dl},$$

$$\text{east} = -\frac{\displaystyle\int_{\partial E}\left(\int_0^{P_{\text{sfc}}} \overline{q}\,\overline{u}\; dp\right) dl}{\displaystyle\int_{\partial E}\left(\int_0^{P_{\text{sfc}}} \overline{q}\; dp\right) dl}$$

$$\text{west} = +\frac{\displaystyle\int_{\partial W}\left(\int_0^{P_{\text{sfc}}} \overline{q}\,\overline{u}\; dp\right) dl}{\displaystyle\int_{\partial W}\left(\int_0^{P_{\text{sfc}}} \overline{q}\; dp\right) dl}. \qquad (6)$$

The preceding quantities measure flow into the sector weighted by moisture. This means that greater moisture bearing levels are given more weight in this new measure of flow. The results for each boundary are averaged, as are the mean specific humidity values, and plotted in Figs. 7a and 7b, respectively. Although variations in specific humidity do show some correlation with variations in MFC, Fig. 7a shows that variations in moisture-weighted flow appear to be primarily responsible for MFC differences between the ERA-15 and TOGA operational series. This suggests that such differences are likely to be manifest in differences of mean geopotential height and flow fields. The next section looks at some analysis differences at 500 hPa. The equivalent baro-

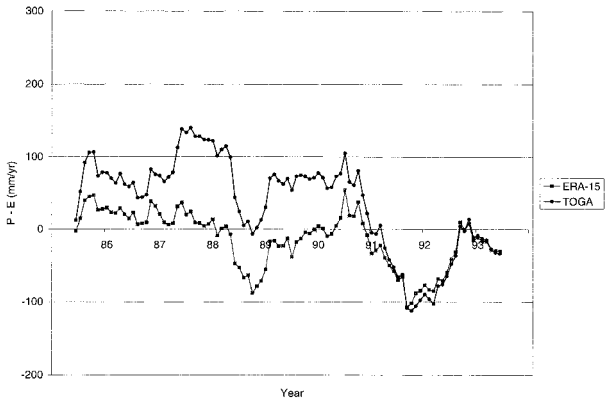

FIG. 6. Annual running mean of the mean zonal (east + west) component of ERA-15 and TOGA MFC to the West Antarctic sector.

tropic nature of the Antarctic atmosphere (Rogers and Van Loon 1982) suggests a high degree of similarity in flow patterns at many levels.

c. 500-hPa differences between analyses and reanalyses

The 500-hPa level is the first standard level completely above Antarctica. Mean conditions at this level are used here to compare/contrast the TOGA operational analyses and ERA-15 over and around the Antarctic continent. Conditions at this level for the period before and after the MFC–SOI correlation switch (circa 1990) are focused on here. The period of the correlation switch also coincides with a change in the mean component (from zonal to meridional) responsible for most of the difference in MFC between the TOGA operational and ERA-15 series.

Figures 8a and 8b are difference plots contrasting the mean 500-hPa geopotential height from TOGA operational analyses and ERA-15 (TOGA minus ERA-15) in the Southern Hemisphere from 50°S to the pole for 1985–90 and 1991–93, respectively. Most prominent in these figures are the large (~20 geopotential meters) mean height differences over East Antarctica and the Southern Ocean. The TOGA operational geopotential heights are consistently greater than those of ERA-15 in these areas. A collaborative investigation with the ERA-15 project team pinpoints the major source of mean field anomaly over the interior of East Antarctica at Vostok station. Here, an error in the ECMWF archived station elevation results in large climatological discrepancies between ERA-15 and radiosonde observations (more in section 4a). A reverse geopotential height pattern is seen over West Antarctica, where ERA-15 heights tend to be higher than those from the TOGA operational analyses. The shape, intensity, and center of this anomaly over West Antarctica changes after 1990 when the MFC–SOI correlation switch occurs and after the departure in agreement between TOGA and ERA-15 mean north component moisture flux contributions (Fig. 5).

Prior to 1990, the mean zonal component of MFC is responsible for most of the discrepancy in total ERA-15 and TOGA operational MFC series (Fig. 6). This discrepancy is reflected in Fig. 8a, which shows that TOGA operational geopotential heights are lower than those of the ERA-15 over the Amundsen Sea coastline and higher over Vostok. This pattern leads to suppressed easterly flow in the ERA-15 and/or enhanced easterly flow in the TOGA operational analyses. Section 4 addresses validation of numerical analyses in these regions of important geopotential height difference.

As demonstrated in Fig. 5, the mean meridional (north boundary) component of MFC is responsible for most of the discrepancy in total ERA-15 and TOGA operational MFC after 1990. Differences in 500-hPa geopotential height in Fig. 8b indicate more northerly flow in the TOGA operational analyses. In Fig. 8a, the area where the ERA-15 geopotential heights are greater than those of the TOGA operational analyses is centered over the coastline bordering the Amundsen Sea. Sandwiched

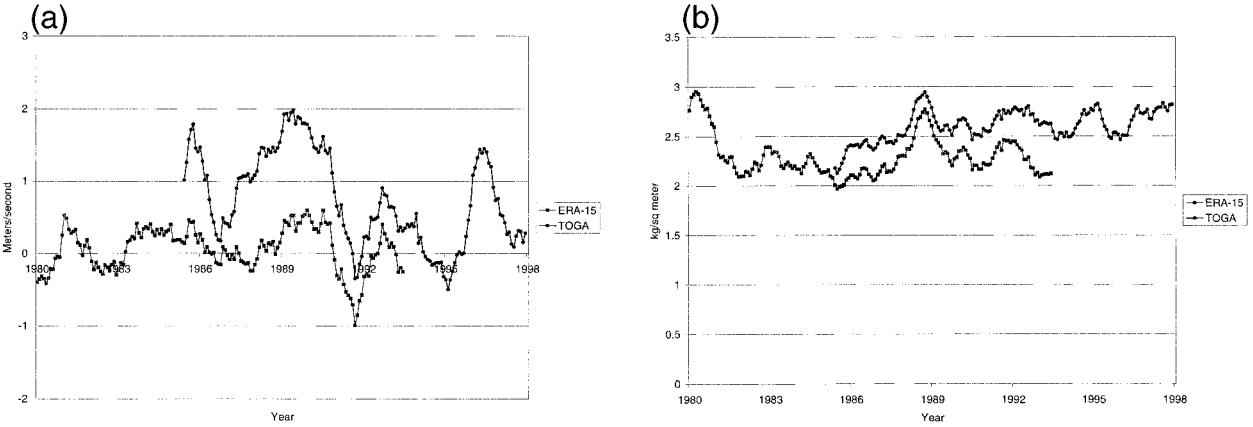

FIG. 7. Boundary average of the annual running means of the (a) mean directional components of MFC divided by vertically and laterally integrated specific humidity and (b) annual running mean precipitable water.

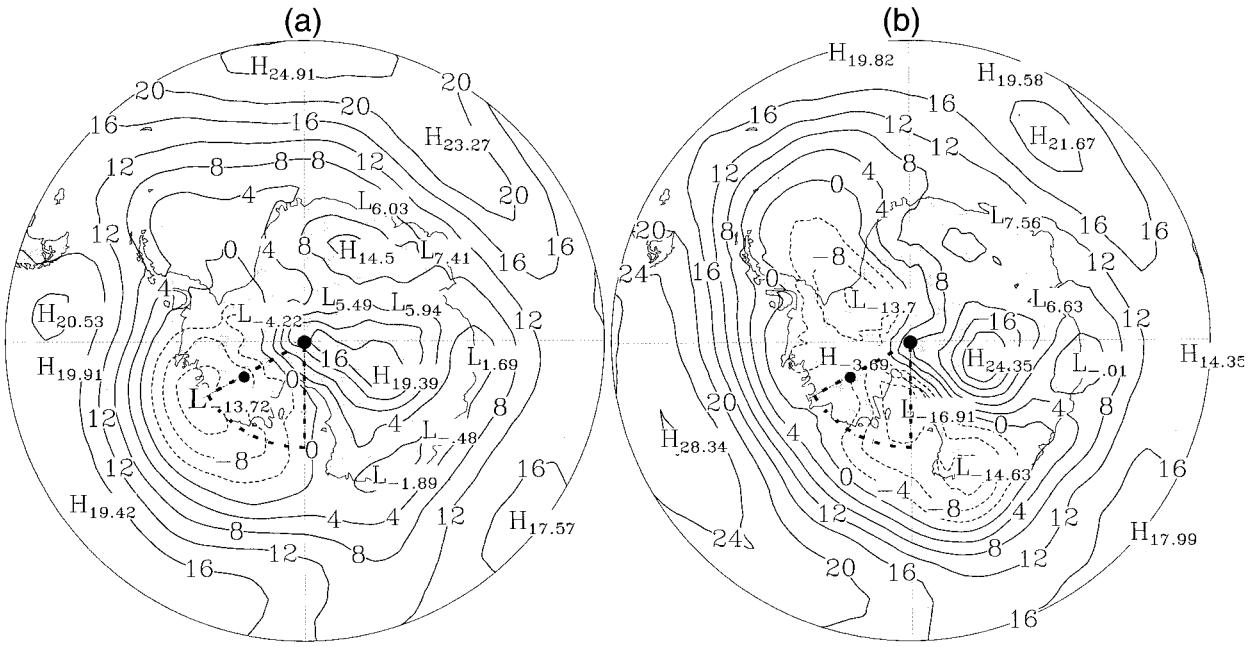

FIG. 8. Difference (TOGA operational minus ERA-15) in 500-hPa mean geopotential height (gpm) for (a) 1985–90 and (b) 1991–93. The dots mark the position of Amundsen–Scott (South Pole) and Byrd stations.

between that height discrepancy and the one centered over Vostok is the eastern boundary of the West Antarctic sector, where most of the discrepancy in MFC is found prior to 1990. Figure 8b reveals that after 1990, the area where ERA-15 geopotential heights are greater than those of the TOGA operational analyses migrates to the Ross Ice Shelf and elongates to encompass an area from the Weddell Sea to the George V Coast in East Antarctica. The resulting geostrophic flow difference across the northern boundary of the West Antarctic sector is manifest through the increase in the mean north components of MFC in Fig. 5. It is thus apparent that differences in MFC to a great extent are related to the mean geopotential height discrepancies, the changing nature of which are relatable to fundamental changes in Antarctic weather patterns around 1990, and not to the resolution increase of the operational analyses that occurs somewhat later. Section 4 looks at observations to help determine the validity of the analyses, before and after 1990.

4. Validation of numerical analyses

Validation using observations is a critical step that must be taken in order to gain confidence in any results obtained from numerical analyses. Bromwich et al. (1995) and Cullather et al. (1997) have done extensive analysis validation of the ECMWF operational data. The purpose of this section is to show how the ERA-15 data perform relative to the validated TOGA operational analyses when compared with observations over and around Antarctica.

a. Comparison of analyses with radiosonde observations

1) 500-hPa geopotential heights and temperatures

Several upper-air stations surrounding the West Antarctic sector are active and report throughout all or most of the TOGA–ERA-15 overlap period. Vostok station (see Fig. 9 for location) in particular shows the greatest overall discrepancy between analyses and observations. The average annual 500-hPa geopotential heights and temperatures from TOGA operational analyses and ERA-15 over Vostok station are subtracted from the average annual radiosonde observations (average observation value minus average analysis value) in Fig. 10. The average analysis values are compiled using specific times when radiosonde data are available. Upper-air information at Vostok station stops very shortly after the start of 1992, so only the period 1985–91 is shown. It is apparent that both analyses tend to produce geopotential heights that are too low and temperatures that are too high. In section 3c, we note that an incorrect station elevation for Vostok in ERA-15 adversely affects analysis production throughout the reanalysis period. The error is of the order of 60 m. It leads to the introduction of a systematic negative bias in the surface pressure analysis, which is also distributed vertically into the lower troposphere at and around the station by the vertical structure function assumed for the mass field in the optimum interpolation (O/I) process (Shaw et al. 1987; Lonnberg 1988). These problems exist at every analysis cycle, since station pressure readings are taken

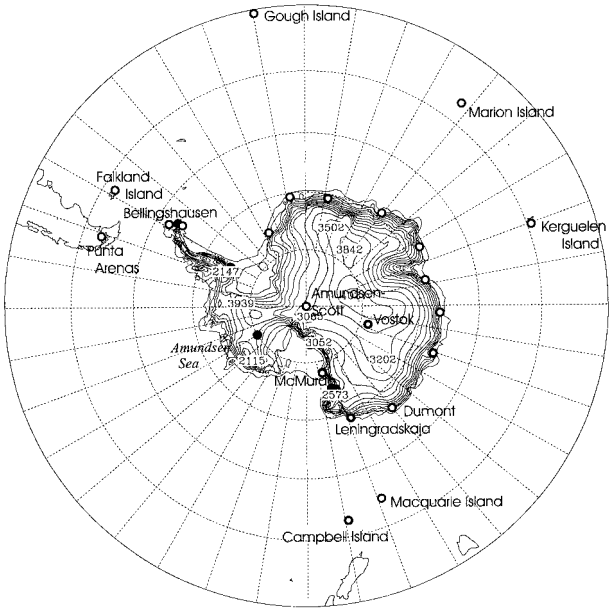

FIG. 9. Map of Antarctica and Southern Ocean from 40°S to the South Pole. Open circles indicate the position of upper-air stations. The lines over Antarctica are elevation contours in 250-m increments.

much more often than radiosondes are launched. The Vostok radiosonde observations themselves are not afflicted by the erroneous archived ECMWF station elevation and thus aid in detecting the error. The same elevation error affects TOGA operational analysis production during the years 1987–90. However, the geopotential height anomaly is not as great during these 4 yr as it is in the ERA-15 (although the 500-hPa temperature during 3 of the 4 yr is better in ERA-15). As described in section 3c, the resultant flow anomaly reduces ERA-15 easterly flow into West Antarctic sector up until the period of the circulation changes (related to the SOI–MFC correlation switch in 1990), evidenced by the mean 500-hPa geopotential height differences in Fig. 8a and the low ERA-15 mean zonal MFC contributions (Fig. 6).

Difference information similar to that displayed in Fig. 10 is computed for Amundsen–Scott (South Pole), Dumont d'Urville, Leningradskaya, McMurdo, and Bellingshausen stations (see Fig. 9 for locations). Overall, the discrepancies (not shown) with observations are not as great as at Vostok. The results indicate that TOGA operational analyses are closer than reanalyses to the annual average radiosonde 500-hPa geopotential heights and temperatures at these continental stations 68% of the time.

Macquarie Island is included in the analysis here to help determine which dataset is closer to observations over the Southern Ocean, the other area where we see large mean differences in geopotential height. This area becomes more important after 1990, when the north component of MFC contributes the most to total MFC. It is also a time when large discrepancies exist between ERA-15 and TOGA mean north component MFC. Similar to Vostok station, the Southern Ocean is an area where TOGA operational 500-hPa analyses often average about 20 geopotential meters higher than ERA-15. As in Fig. 10, annual differences of Macquarie Island 500-hPa geopotential heights and temperatures (observation minus analysis value) are plotted in Figs. 11a and 11b, respectively. TOGA operational heights are 10–14 geopotential meters low compared with observed values, whereas ERA-15 heights are 16–25 geopotential meters low. In addition, it seems that where there are Southern Ocean upper-air stations (e.g., Macquarie Island, Kerguelen Island, Marion Island, Gough Island, etc.; Fig. 9), the differences between analyses are generally less than half those over observation-void Southern Ocean regions. The Macquarie Island geopotential height results suggest that, in such data-void regions where the ERA-15 heights are ~20 geopotential meters lower than the TOGA operational values, the reanalysis 500-hPa heights are much lower than the actual 500 hPa

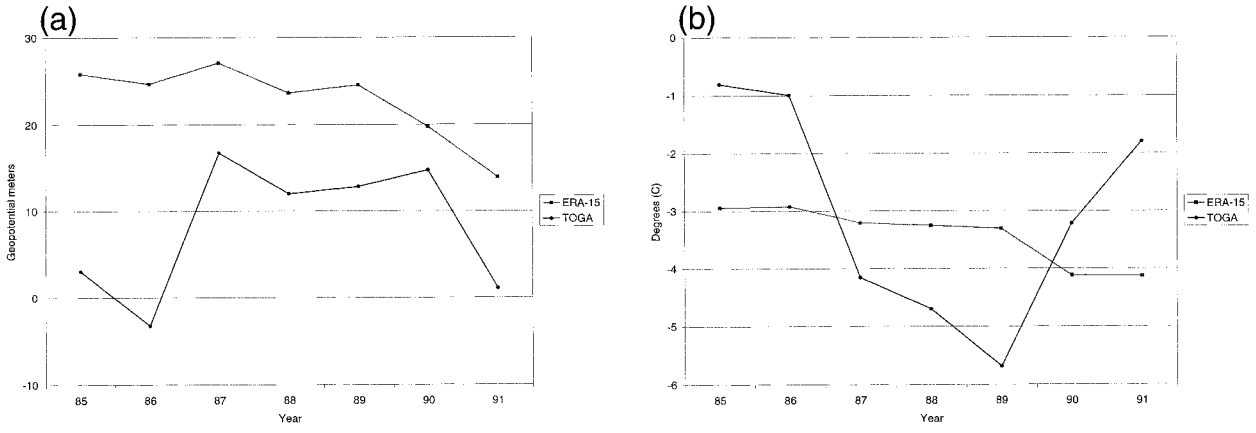

FIG. 10. Difference of annual mean radiosonde observations and analyses (observations minus analyses) for 500-hPa (a) geopotential heights and (b) temperatures at Vostok station.

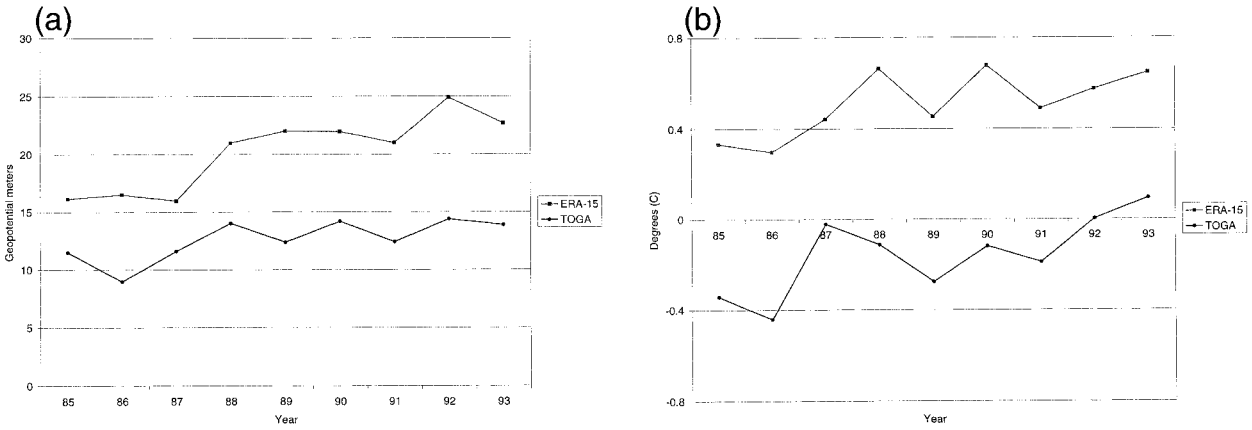

FIG. 11. Difference of annual mean radiosonde observations and analyses (observations minus analyses) for 500-hPa (a) geopotential heights and (b) temperatures at Macquarie Island.

geopotential heights. The 500-hPa temperature differences between observations and analyses at Macquarie Island are quite small. TOGA operational analyses are slightly warm (~0.15°C), whereas ERA-15 500-hPa temperatures are too cool (~0.5°C). Even if analysis temperatures at the surface start out the same and are different by 0.65°C at 500 hPa, the effect on geopotential height is of the right magnitude to explain the difference between the analyses in Fig. 11a. Kållberg (1997) notes that the ERA-15 assimilation warms the atmosphere below 300 hPa at higher latitudes. In other words, the ERA-15 first guess has a cold bias when compared with radiosondes in this region.

These results show that the reanalyses are in general less close to the radiosonde measurements than the operational ECMWF analyses in the TOGA dataset. It is likely that these results are due to the use of many other kinds of data in ERA-15. In particular, TOVS CCRs are used in the 1D-Var process. 1D-Var has a major impact on ERA-15, particularly over otherwise data-sparse and data-void areas such as the Southern Ocean. In the older TOGA analyses, TOVS data were used in the form of low-resolution SATEM retrievals. The inclusion of more data of different types in the O/I assimilation process in ERA-15 forced the resulting analyses to become an optimized compromise between the different observation types and the assimilating forecast model. Operational experience at ECMWF indicates that analyses using 1D-Var retrievals, such as are used in ERA-15, produce superior short- and medium-range forecasts compared to the older analyses available in the TOGA set, particularly in the Southern Hemisphere. Thus, reanalyses may not always fit as closely to the radiosonde data as operational analyses based on fewer competing data—as we see in the present context. At least from the perspective of the present climate study, a smaller *average* difference between 0-h hour (re)analyses and in situ observations is preferable to optimizing forecast results at the expense of the 0-h analyses.

The result of reanalysis differences with radiosonde observations appears to have had an influence on mean north component MFC, which is significantly lower than that of the TOGA operational series during the post-1990 period. How low ERA-15 MFC values are related to discrepancies with radiosonde observations is even more apparent when we look at analysis vertically integrated moisture at coastal stations.

2) VERTICALLY INTEGRATED MOISTURE AT MCMURDO AND BELLINGSHAUSEN STATIONS

Although accurately measuring atmospheric moisture content in the cold and dry region of Antarctica can be difficult (especially in the interior), a limited analysis of atmospheric moisture at two coastal stations is included here as another means of numerical analysis validation. Annual running mean vertically integrated precipitable water is calculated for McMurdo (Fig. 12a) and Bellingshausen (Fig. 12b) stations using average monthly radiosonde and analysis data. These are the closest coastal stations to the West Antarctic sector for which MFC is computed. The results are consistent in both plots. In general, numerical analyses are not as moist as they should be based on radiosonde observations. Of the two numerical analysis series plotted, the TOGA series comes closest to the values obtained from radiosonde data. At McMurdo, calculations yield a mean radiosonde value of 2.7 kg m^{-2}, a mean TOGA value of 2.0 kg m^{-2} (26% below that observed), and a mean ERA-15 value of 1.4 kg m^{-2} (46% below that observed). Standard errors of the mean monthly values are 1.3, 1.3, and 1.2 kg m^{-2} using radiosonde, TOGA, and ERA-15 data, respectively. At Bellingshausen, calculations yield a mean radiosonde value of 8.4 kg m^{-2}, a mean TOGA value of 8.2 kg m^{-2} (3% below that observed), and a mean ERA-15 value of 7.1 kg m^{-2} (16% below that observed). Standard errors of the mean monthly values are 0.2, 0.3, and 0.4 kg m^{-2} using radiosonde, TOGA, and ERA-15 data, respectively. These results indicate that the TOGA operational analyses come closer to giv-

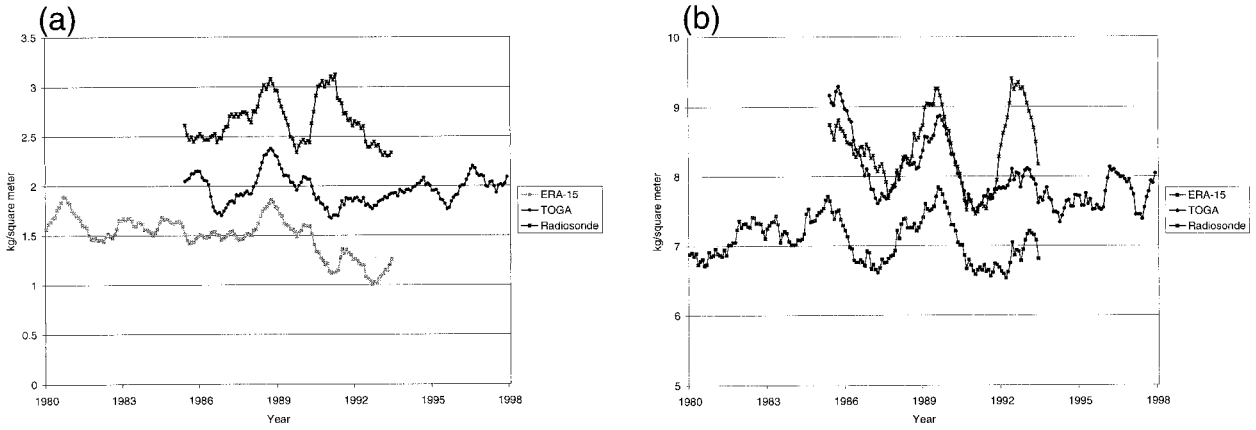

FIG. 12. Annual running mean of vertically integrated moisture at (a) McMurdo and (b) Bellingshausen.

ing an accurate representation of atmospheric moisture content than the ERA-15 at these coastal stations. While variations in atmospheric moisture content appear to play a secondary role in MFC for the West Antarctic sector (i.e., variations in MFC are primarily determined by atmospheric flow as seen in section 3b), persistent low moisture values in ERA-15 data help to explain part of the difference in mean northerly MFC values after 1990.

b. Byrd AWS pressure variability and Phillpot results

West Antarctica is the one area in the Southern Hemisphere where ERA-15 500-hPa geopotential heights tend to be higher than those of the TOGA operational analyses. Unfortunately, there are minimal amounts of upper-air data in this area, especially near the West Antarctic sector where MFC is calculated. The Phillpot technique (Phillpot 1997) is used to estimate 700-hPa geopotential heights over the Byrd automatic weather station (AWS) in West Antarctica (80.0°S, 119.4°W; Fig. 1) from surface pressure and temperature observations as a means of validating ERA-15 and TOGA operational analyses. In addition, pressure variability at the Byrd AWS is also checked in the analyses. The results using the Phillpot technique are shown in Fig. 13.

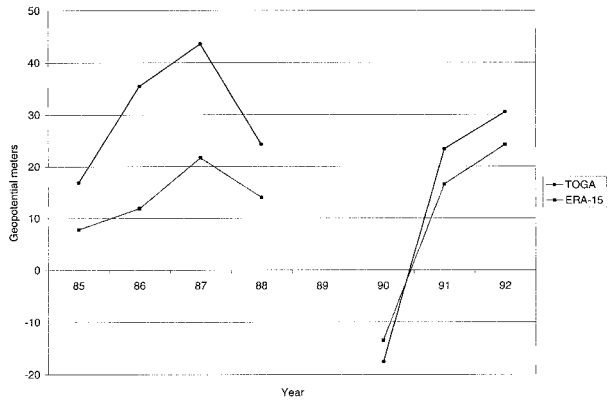

FIG. 13. Difference of annual mean 700-hPa geopotential heights for Byrd AWS calculated using the Phillpot technique and for analyses (observations minus analyses).

There are no viable data at the Byrd AWS for most of 1988–89. After this period of no observations, ERA-15 and TOGA operational analyses perform equally well with regards to pressure variability (both greater than 0.90 correlation with AWS pressure) and almost equally well in 700-hPa geopotential heights in Fig. 13. However, from 1985 to the beginning of 1988, reanalyses are closer to observations than TOGA operational analyses in both pressure variability and (estimated) geopotential height comparisons. Given the difficulties in data transmission known to exist in this region at times, it is possible that a portion of the TOGA operational departures from observation seen in the late 1980s are the result of data transmission difficulties resulting in a lack of observations for operational analysis production. However, this region is not located in the center of the negative TOGA operational minus ERA-15 West Antarctic geopotential height anomaly seen in Fig. 8a.

In section 3, it is noted that geopotential height differences over both Vostok Station in East Antarctica and over the Amundsen Sea coastline in West Antarctica contribute to differences in the magnitude of mean easterly flow into the West Antarctic sector. While the low reanalysis geopotential heights over Vostok occur as a result of an erroneous archived station elevation, evidence at the Byrd AWS suggests that higher ERA-15 geopotential heights centered over the Amundsen Sea coastline may be closer to the actual heights than the TOGA operational analyses. However, this may be an instance where spatial consistency in analysis shortcomings is more desirable than a very localized large geopotential height discrepancy. To test this, an average geopotential height field is calculated using data from 1957 (the International Geophysical Year) through 1966, years that correspond with the collection of upper-air data at Byrd station and a number of West Antarctic

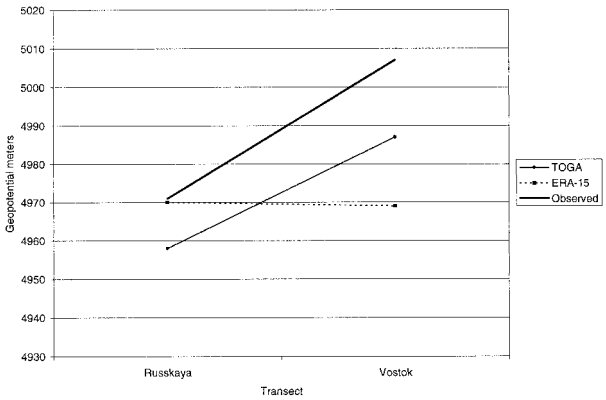

FIG. 14. The 500-hPa geopotential heights near Russkaya and Vostok stations using climatological data from 1957 to 1966 along with heights obtained using numerical analyses for the period 1985–90.

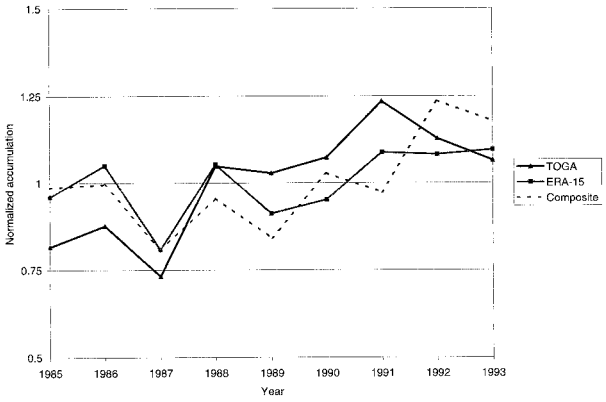

FIG. 15. Normalized values of TOGA and ERA-15 annual MFC values plotted with a normalized linear average of ice-core accumulation data from Byrd and Siple Dome.

coastal stations. The mean 500-hPa geopotential height field obtained from these data (Taljaard et al. 1969) is subsequently adjusted to compensate for errors in recorded elevation during this early period at Vostok, Amundsen–Scott (Schwerdtfeger 1981), and Byrd stations. Then, 500-hPa geopotential heights near Russkaya (along the Amundsen Sea coastline) and Vostok stations are obtained and compared with numerical analysis values at the same points for the years 1985–90. This period corresponds with the large differences between TOGA and ERA-15 MFC across the eastern boundary of the domain. The results (Fig. 14) show that the TOGA operational analyses have a spatial trend similar to the one obtained from the relatively dense network of upper-air stations that existed through the region from 1957–66. On the other hand, ERA-15 500-hPa geopotential height across the Russkaya–Vostok transect does not increase as it does in the observations and in the TOGA operational depiction, resulting in the reanalyses having almost no mean easterly flow across the eastern boundary of the West Antarctic sector.

c. Ice-core analyses

1) ACCUMULATION DATA FROM BYRD STATION AND SIPLE DOME

Ice cores taken from near Byrd station and Siple Dome (see Fig. 1) are used to look for trends and variability in West Antarctic sector precipitation for the period that ERA-15 and TOGA operational analyses overlap. The three ice cores near Byrd station are from locations (78.73°S, 116.33°W; 79.46°S, 118.05°W; and 80.01°S, 119.56°W) along a 150 km north-northeast to south-southwest line with Byrd station at the south-southwestern end. The three ice cores from the summit area of Siple Dome (near the eastern edge of the Ross Ice Shelf in Fig. 1) are from locations 81.68°S, 149.19°W; 81.64°S, 148.77°W; and 81.71°S, 148.60°W. All cores are dated with two independent techniques and yield annual estimates of accumulation rate (Kreutz et al. 2000, manuscript submitted to *Geophys. Res. Lett.*). For each location the three records are averaged to mitigate the spatial accumulation variability that characterizes polar ice sheets.

Upon calculating a linear average of the Byrd station and Siple Dome annual accumulation results, this series is normalized by dividing by the mean annual value and compared with similarly normalized ERA-15 and TOGA annual $P - E$ values (Fig. 15). From the late 1980s to the early 1990s, there is a significant increase in TOGA operational MFC (a total of 30% from the beginning to the end of the period shown). Although ERA-15 MFC is slightly higher in 1993 than in 1985, the increase is less than half that seen in the TOGA series. The tendency of accumulation from core data (up 20%) falls between those seen in the TOGA and ERA-15 series. The plot also shows that there is general agreement in interannual variability among the series (the notable exception is the year before and after 1991).

The core data are obtained in areas that are relatively dry for the West Antarctic sector, averaging roughly half the total sector precipitation obtained from ECMWF numerical analyses. Much larger amounts of precipitation are known to fall over the marginal ice slopes of the West Antarctic sector near the Amundsen Sea (Giovinetto and Bentley 1985; Vaughan et al. 1999). For instance, the spatial trend of low mean precipitation near Byrd to greater amounts farther north toward the coast is evidenced by the northernmost ice core near Byrd, which shows almost twice the mean accumulation as the other two ice cores farther inland. Thus, from our results we can conclude that the core accumulation data tend to support the interannual variability seen in both of the numerical depictions presented. However, while both numerical $P - E$ and ice accumulation results portray an upward trend in net precipitation, additional cores from the higher accumulation regions nearer the coast are needed to determine whether an observationally based upward trend lends more support to the larger

positive trend obtained from TOGA analyses or to the smaller one from ERA-15.

2) Isotope analysis of a Siple Dome ice core

Deuterium isotope concentrations from ice-core analyses serve as a proxy for variations of moisture flux convergence into the West Antarctic sector and should be correlated with ENSO events. The reason for this is due primarily to the positioning of the low pressure center in the Amundsen Sea and to a relationship between isotopic concentration and distance from the primary moisture source (Bromwich and Weaver 1983). Previously, a case study by Chen et al. (1996) showed how ENSO cycles are probably linked to the Amundsen Sea low via signal propagation along the South Pacific convergence zone. In addition, a more recent study by Marshall and King (1998) showed that interannual variations in the intensity of low pressure in the Amundsen Sea are related to ENSO and impact Antarctic Peninsula temperatures. As demonstrated in Fig. 5 of C96, the center of Amundsen Sea low pressure during normal precipitation events (e.g., 1980) is located just north of the Ross Ice Shelf. During reduced precipitation events (e.g., 1982), the center of this low migrates to the far eastern side of the Amundsen Sea. The impact on vertically integrated moisture flux (also plotted in Fig. 5 of C96) shows that the flow during normal precipitation events is meridional and more direct than during reduced events, at which time the flow is more from the east across the sector, suggestive of dryer and cooler conditions. Month-to-month variations in isotope concentrations of polar precipitation are primarily determined by the condensation temperature contrast between moisture source and precipitation location (Dansgaard 1964), with higher isotope concentrations occurring under warmer conditions. Thus, we expect the less direct, cooler flow to the West Antarctic sector indicated in the low precipitation events to be reflected in low deuterium isotope levels. Likewise, more direct, moister, and warmer flow from the Ross Sea during higher, or more normal, precipitation events should be reflected by higher isotopic concentrations of deuterium.

Figure 16 shows depletion values of deuterium isotopes obtained from the subannually dated Siple Dome B ice core (81.5263°S, 148.8139°W) plotted with the SOI (both as annual running means). It is important to note that isotope concentrations obtained from ice cores are naturally smoothed by vapor diffusion in the snowpack. This process leads to more smoothing in the earlier part of the series than in the later part, so a Gaussian low-pass filter was applied to the more recent portion of the isotope series. Frequencies higher than one cycle per 18 months are smoothed away, simulating the vapor diffusion that has already removed higher frequencies in the earlier portion of the series. The plot indicates the same correlation pattern as is seen between MFC and the SOI in Fig. 2. The correlation switch from positive to negative happens at the same time as with MFC, circa 1990. The series in Fig. 16 even show some evidence of another switch occurring around the time of the 1982–83 ENSO event, from being negatively to positively correlated. This is reflected in a comparison between the SOI and the WMO and ERA-15 series in Figs. 2 and 3, respectively. However, there are only 2–3 yr available with which to see the antiphase relationship that appears to exist prior to 1982.

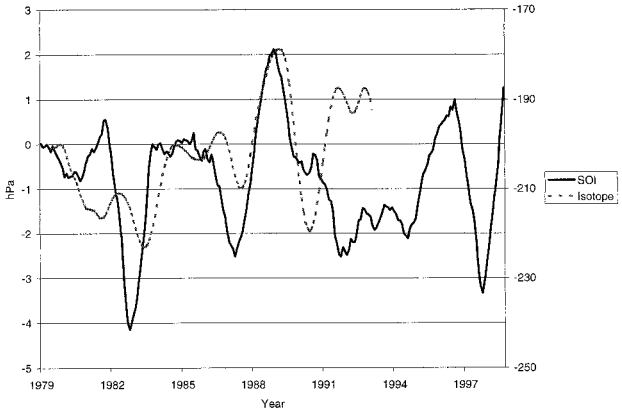

FIG. 16. Annual running mean of deuterium isotope depletions obtained from Siple Dome ice-core analysis (right scale in per mil) and the SOI (left scale).

It is important to note that these results are from one ice core. Several additional cores will be drilled in this area, sampling over a greater area, which will help determine the fidelity of this isotope–SOI relationship once the spatial coverage of sampling is enhanced. However, this isotope analysis provides convincing glaciochemical support of the strong West Antarctic sector MFC–SOI correlation pattern seen in the TOGA operational analyses. The results also illustrate the value of diverse information sources for validation in this data sparse area.

5. Discussion

Discrepancies in MFC between the ECMWF operational analyses and those of ERA-15 in the West Antarctic sector from the mid-1980s through the early 1990s are almost entirely the result of differences in the mean components of MFC across the boundaries. From the middle to the end of the 1980s, the mean component of MFC across the eastern boundary explains most of the difference seen in total MFC for the sector. In the early 1990s, the mean component of MFC across the northern boundary is most responsible for the difference. In each instance, the differences in mean moisture flux at the boundaries are reflected in mean flow and geopotential height differences. A difference plot of the ERA-15 and TOGA operational analysis mean geopotential height field reveals a spatially and temporally steady height anomaly with operational analyses averaging ~20 gpm

higher over the southeastern Pacific and East Antarctica (centered over Vostok station), and the ERA-15 averaging ~10 gpm higher over West Antarctica.

An error in the recorded elevation of Vostok in the ERA-15 results in analysis geopotential height and wind differences with the TOGA archive that effectively damp ERA-15 easterly flow into the West Antarctic sector. Atmospheric flow is shown to be the mechanism that most impacts MFC to the West Antarctic sector. Although ERA-15 700-hPa geopotential heights are closer to Phillpot calculations over Byrd AWS than the early part of TOGA operational analyses from 1985 to 1988, mean spatial tendencies of the height field are found to be the most important factor for MFC calculations. The low Vostok reanalysis geopotential heights result in a flat geopotential height field from East Antarctica through Byrd station and out over the Amundsen Sea. Both observations and TOGA operational analyses show that Vostok heights should be higher than those over the Amundsen Sea coastline near Russkaya station, ultimately resulting in mean flow into the West Antarctic sector across the eastern boundary.

Comparisons with radiosonde data near the West Antarctic sector show that the ERA-15 analyses are less constrained by radiosonde observations at high southern latitudes than the ECMWF operational analyses, especially over the Southern Ocean and interior of East Antarctica. The ultimate result is manifested as lower overall sensitivity to ENSO signals in the ERA-15 Antarctic analyses. This finding demonstrates the need for prudent validation efforts using available observations and other information in order to ascertain the applicability of numerical (re)analyses.

Given the emphasis placed on validating numerical analyses using in situ observations, it should be noted that the differences between numerical analyses and observations in this study are temporal averages. For a particular time and place, we expect some difference between analyses and observations for many reasons including spatial resolution. However, temporal averaging should mitigate this contrast, leaving biases, which can have a negative impact on mean fields, as demonstrated in this paper.

Prior results obtained by C96 that show a strong correlation of West Antarctic sector precipitation with the SOI, as well as an upward trend in precipitation, are based on ECMWF operational analyses, which are in good agreement with the observations. The positive-to-negative SOI–MFC correlation switch that occurs around 1990 is substantiated by an updated MFC series that continues to show a strong negative correlation through the current period (beginning of 1999). West Antarctic sector ice cores confirm an upward trend in precipitation accumulation for the period over which the ERA-15 and TOGA operational analyses overlap (1985–93). A Siple Dome deuterium isotope record (serving as a proxy for West Antarctic sector MFC) yields the same interannual variability pattern with the SOI as the MFC series, further validating the existence of the ENSO teleconnection in the West Antarctic sector. Based on these findings, more research is needed to understand the changing correlation pattern between West Antarctic sector precipitation accumulation and the SOI. Additional forcings from the tropical Indian Ocean (Quintanar and Mechoso 1995) and from Antarctica (Chen et al. 1996; Quintanar and Mechoso 1995) will need to be considered in order to understand more fully the changing nature of this low-to-high–southern latitude teleconnection.

Acknowledgments. This research is supported by National Science Foundation Grants OPP-9420681 and OPP-9725730 and by National Aeronautics and Space Administration Grant NAG5-6001. Numerical analysis data were supplied by NCAR.

REFERENCES

Angell, J. K., 1981: Comparison of variations in atmospheric quantities with sea surface temperature variations in the equatorial eastern Pacific. *Mon. Wea. Rev.,* **109,** 230–243.

Bromwich, D. H., 1988: Snowfall in high southern latitudes. *Rev. Geophys.,* **26,** 149–168.

——, and C. J. Weaver, 1983: Latitudinal displacement from main moisture source controls $\delta^{18}O$ of snow in coastal Antarctica. *Nature,* **301,** 145–147.

——, F. M. Robasky, R. I. Cullather, and M. L. Van Woert, 1995: The atmospheric hydrologic cycle over the Southern Ocean and Antarctica from operational numerical analyses. *Mon. Wea. Rev.,* **123,** 3518–3538.

——, R. I. Cullather, and M. L. Van Woert, 1998: Antarctic precipitation and its contribution to the global sea level budget. *Ann. Glaciol.,* **27,** 220–226.

Budd, W. F., P. A. Reid, and L. J. Minty, 1995: Antarctic moisture flux and net accumulation from global atmospheric analyses. *Ann. Glaciol.,* **21,** 149–156.

Chen, B., S. R. Smith, and D. H. Bromwich, 1996: Evolution of the tropospheric split jet over the South Pacific Ocean during the 1986–89 ENSO cycle. *Mon. Wea. Rev.,* **124,** 1711–1731.

Cullather, R. I., D. H. Bromwich, and M. L. Van Woert, 1996: Interannual variations in Antarctic precipitation related to El Niño–Southern Oscillation. *J. Geophys. Res.,* **101,** 19 109–19 118.

——, ——, and R. W. Grumbine, 1997: Validation of operational numerical analyses in Antarctic latitudes. *J. Geophys. Res.,* **102,** 13 761–13 784.

——, ——, and M. L. Van Woert, 1998: Spatial and temporal variability of Antarctic precipitation from atmospheric methods. *J. Climate,* **11,** 334–368.

Dansgaard, W., 1964: Stable isotopes in precipitation. *Tellus,* **16,** 436–468.

Genthon, C., and A. Braun, 1995: ECMWF analyses and predictions of the surface climate of Greenland and Antarctica. *J. Climate,* **8,** 2324–2332.

——, and G. Krinner, 1998: Convergence and disposal of energy and moisture on the Antarctic polar cap from ECMWF reanalyses and forecasts. *J. Climate,* **11,** 1703–1716.

Gibson, J. K., P. Kållberg, S. Uppala, A. Hernandez, A. Nomura, and E. Serrano, 1997: ERA Description. ECMWF Re-analysis Project Report Series, Part 1, ECMWF, 72 pp.

Giovinetto, M. B., and C. R. Bentley, 1985: Surface balance in ice drainage systems of Antarctica. *Antarct. J. U.S.,* **20** (4), 6–13.

Gloersen, P., 1995: Modulation of hemispheric sea-ice cover by ENSO events. *Nature,* **373,** 503–506.

Houseago, R. E., G. R. McGregor, J. C. King, and S. A. Harangozo,

1998: Climate anomaly wave-train patterns linking southern low and high latitudes during South Pacific warm and cold events. *Int. J. Climatol.,* **18,** 1181–1193.
Kallberg, P., 1997: Aspects of the Re-analysed Climate. ECMWF Re-Analysis Project Report Series, Part 2, ECMWF, 89 pp.
Ledley, T. S., and Z. Huang, 1997: A possible ENSO signal in the Ross Sea. *Geophys. Res. Lett.,* **24,** 3253–3256.
Lettau, B., 1969: The transport of moisture into the Antarctic interior. *Tellus,* **21,** 331–340.
Lonnberg, P., 1988: Developments in the ECMWF analysis system. *Proc. ECMWF Seminar on Data Assimilation and the Use of Satellite Data,* Vol. 1, Reading, United Kingdom, ECMWF, 75–119.
Marshall, G. J., and J. C. King, 1998: Southern Hemisphere circulation anomalies associated with extreme Antarctic Peninsula winter temperatures. *Geophys. Res. Lett.,* **25,** 2437–2440.
Phillpot, H., 1997: Some observationally-identified meteorological features of East Antarctica. Bureau of Meteorology Meteorological Study 42, 275 pp. [Available from Bureau of Meteorology, GPO Box 1289K, Melbourne, VIC, 3001, Australia.]
Quenouille, M. H., 1952: *Associated Measurements.* Butterworths, 241 pp.
Quintanar, A. I., and C. R. Mechoso, 1995: Quasi-stationary waves in the Southern Hemisphere. Part I: Observational data. *J. Climate,* **8,** 2659–2672.
Renwick, J. A., 1998: ENSO-related variability in the frequency of South Pacific blocking. *Mon. Wea. Rev.,* **126,** 3117–3123.
Rogers, J. C., and H. van Loon, 1982: Spatial variability of sea level pressure and 500 mb height anomalies over the Southern Hemisphere. *Mon. Wea. Rev.,* **110,** 1375–1392.
Schwerdtfeger, W., 1981: Elevation of Amundsen–Scott South Pole Station: 2,835 meters. *Antarct. J. U.S.,* **16** (4), 10–11.
Shaw, D. B., P. Lonnberg, A. Hollingsworth, and P. Undèn, 1987: Data assimilation: The 1984/85 revision of the ECMWF mass and wind analysis. *Quart. J. Roy. Meteor. Soc.,* **113,** 533–566.
Simmonds, I., and T. H. Jacka, 1995: Relationships between the interannual variability of Antarctic sea ice and the Southern Oscillation. *J. Climate,* **8,** 637–647.
Stone, R., 1997: Storm aborts Antarctic drilling project. *Science,* **278,** 1007–1008.
Taljaard, J. J., H. van Loon, H. L. Crutcher, and R. L. Jenne, 1969: *Climate of the Upper Air: Part 1—Southern Hemisphere.* Vol. 1, *Temperatures, Dewpoints, and Heights at Selected Pressure Levels,* Naval Weather Service Command, 144 pp.
Trenberth, K. E., 1992: Global analyses from ECMWF and atlas of 1000 to 10 mb circulation statistics. NCAR Tech. Note NCAR/TN-373+STR, 191 pp. and 24 fiche.
——, and T. J. Hoar, 1996: The 1990–1995 El Niño–Southern Oscillation event: Longest on record. *Geophys. Res. Lett.,* **23,** 57–60.
Vaughan, D. G., J. L. Bamber, M. Giovinetto, J. Russell, A. Paul, and R. Cooper, 1999: Reassessment of net surface mass balance in Antarctica. *J. Climate,* **12,** 933–946.
White, W. B., and R. G. Peterson, 1996: An Antarctic circumpolar wave in surface pressure, wind, temperature and sea-ice extent. *Nature,* **380,** 699–702.
Yamazaki, K., 1992: Moisture budget in the Antarctic atmosphere. *Proc. NIPR Symp. Polar Meteor. Glaciol.,* **6,** 36–45.